environmental sciences proceedings

MDPI

Proceeding Paper

An Attempt: Modified Semi-empirical Approach Based to Retrieve Soil Fluoride Using Sentinel-1 SAR Data over Agricultural Patches

Vijayasurya Krishnan and Manimaran A *

Department of Civil Engineering, Faculty of Engineering and Technology, SRM Institute of Science and Technology, Kattankulathur 603 203, Chengalpattu District, Tamilnadu, India; vk9075@srmist.edu.in

* Correspondence: manimara@srmist.edu.in

† Presented at the 5th International Electronic Conference on Remote Sensing, 7–21 November 2023; Available online: https://ecrs2023.sciforum.net/.

Abstract: Plant growth and its health are affected by 0.06 – 0.09% crustal fluoride. A semi-empirical model estimated wet soil fluoride using Sentinel-1 5.405 GHz data as dependent on dielectric components and loss angles. Mineral surface charges and electrical potential limit clay soil ion mobility via moisture and permeability. Real and imaginary dielectric components approximate 3° to 4° loss angle in lab soil samples with high and low fluoride electrical conductivity. An estimated percentage of dielectric component loss over wide areas may imply fluoride. Finally, linear regression between field fluoride value and conductance loss estimate fluoride. The statistical differences (R^2 = 0.86, RMSE = 1.90, and Bias = 0.35) between predicted and simulated fluoride levels over clay soil and soil with different vegetation development suggest C-band SAR data may detect fluoride.

Keywords: soil moisture; imaginary part of dielectric constant; loss tangent; saline associated fluoride; and soil pH

1. Introduction

An Earth's crust contains 0.1 % fluoride and it's constituent. Among that, 85 million tonnes of fluoride deposits are in the earth's crust worldwide, and from that 12 million tonnes are found in India[1]. (Singh et al., 2018) investigated that In India, > 62 million people in almost twenty states are facing problems due to fluoride ion (F^-) [2]. Initially, soil-related studies (moisture, texture, temperature and roughness) are carried out several research in the laboratory by taking field samples. In the next stage, based on the initial work the laboratory instruments are modified according to the field conditions to collect the real-time data [3–5]. However, for large-scale studies, the laboratory tests are limited to varying soil conditions from region to region, and the obtained result cannot apply to other field conditions. Hence as an alternative, a remote sensing technology was adopted to overcome the limitation of the above problem.

Researchers used optical remote sensing to map soil characteristics using sensitivity-based indices. Empirical models or indices: Perpendicular Drought Index (PDI) and Temperature Vegetation Dryness Index (TVDI), Noah- land surface model (LSM), Normalized difference turbidity index (NDTI), and Palmer Drought Severity Index (PDSI), modified perpendicular drought index (MPDI), Normalized Multi-band Drought Index (NMDI) and a systematic scientific theorem [6–8]. For past 30 years, geologic remote sensing has employed Landsat TM pictures to map lithology and lineaments, specifically mineralogy and iron oxide ratio. The Landsat TM band 7 to band 5 ratio is utilised to distinguish argillic and non-argillic materials because it demonstrates hydroxyl absorption band sensitivity. The band-based methods were accurate for very salty soils,

Citation: To be added by editorial staff during production.

Academic Editor: Firstname Lastname

Published: date

whereas less salty soils were drawn with intermediate accuracy and improved with fuzzy boundaries. Recently, automated image classification on learning selection using soil imagery and salinity index values was used to create salinity maps. One of the main limitations of optical remote sensing is that it introduces more climatic uncertainty and also, penetrates the soil subsurface poorly.

Thus, microwave remote sensing was used in soil research since it is unaffected by environmental conditions and provides extensive information due to its penetration. The small perturbation model (SPM), integral equation model (IEM), Advanced Integral Equation Model (AIEM), semi-empirical water cloud model, and Michigan Microwave Canopy Scattering model (MIMICS) all measure soil moisture, but they are limited to flat terrain soil, surfaces covered in different materials, and more field parameters [9-11]. Instead, [Lievens and Verhoest] and [Zhou] added vegetation characteristics to the water cloud model to eliminate vegetation and improve accuracy.

Thus, numerous techniques have been created to illustrate that soil dielectric constant (DC) depends on volumetric moisture content and textural composition (Wang et al., 1986). Dobson's model initially proposed a soil moisture-dielectric constant relationship, however, it failed to separate bound and bulk water. The Mirnov proposed transition moisture to circumvent this limitation, but it was susceptible to excessive sand content [12]. To circumvent the limitations of both approaches, the Density Space Dielectric Model (DSDM) was created to distinguish saline soil from non-saline soil by considering soil texture as a function of moisture and polarization [13]. Limiting to individual salt elements, a well-established relationship between the dielectric constant and total salt levels in the imaginary section estimates soil water system dielectric loss (Sreenivas et al., 1995, Xiang and Shao, 2006). The study's model (Jacob V M, 2005) derived fluoride components from dielectric tangent loss by connecting the real and imaginary ($\epsilon_{i)}$ components of the dielectric constant [14].

The objective of this study is as follows: (i) To evaluate the performance of ISVI in soil moisture evaluation. (ii) To evaluate the performance of the Soil Textural Index considering ISVI-based soil moisture. (iii) In this current study proposed a modified approach to estimate the Fluoride in soil.

2. Material and Methods

2.1. Study Area and Data Feasibility

The Perambalur district is in southern India, in the centre of Tamilnadu between 10° 54' and 11° 30' N and 78° 40' and 79° 30' E. The southern plateau district has semi-arid weather, moderate moisture, and geological conditions are similar to worldwide black granite. Agriculture accounts for nearly half of the district's 93,581 Ha and the cultivated area to mobilise fluoride. The district's soil is red loamy and black with substantial clay concentration, covering 943.83 square kilometres or 53% of the total area. According to the 2019-20 report, fertiliser application is 16,627 Metric Tons, soil fertility is extremely poor, and organic carbon is moderate to high alkaline.

This study collected synthetic aperture radar sentinel-1 of Interferometric Wide-Swath Mode (IW) C-band data with dual polarisation on 04 March 2022, matching field observations. This study uses a sentinel-1 with a 12-day return interval and a Level-1 ground range (GRD) format with a spatial resolution of 10 m. (Filipponi 2019) details the processes of radiometric calibration, speckle filtering, and Range-Doppler terrain correction are carried out.

Salinity and fluoride in the soil are harmful to crops, especially mid-stage. Therefore, field surveys were done during cropping. To maintain field conditions, soil and water samples from 165 sites were kept in zip-lock bags and 30 percent of the samples considered for validation. The soil moisture kit measured volume percentage at 5 cm depth. Laboratory tests assess electrochemical parameters such as electrical conductivity (EC), pH, and fluoride content after site sample collection [15,16]. A Conical Flask Shaker

mixes a soil sample at room temperature of 24 ± 2°C with a 1:5 soil-field water ratio for over 30 minutes. Finally, a conductivity probe coupled to a pH/EC Metre, network analyzer at 4 to 6 GHz frequency, and Spectrophotometer measured EC, pH, dielectric components, [13] and fluoride. The laboratory research showed that water bodies in Perambalur lose more fictitious water due to water obtained from varied soil and mineral sources to agricultural patches.

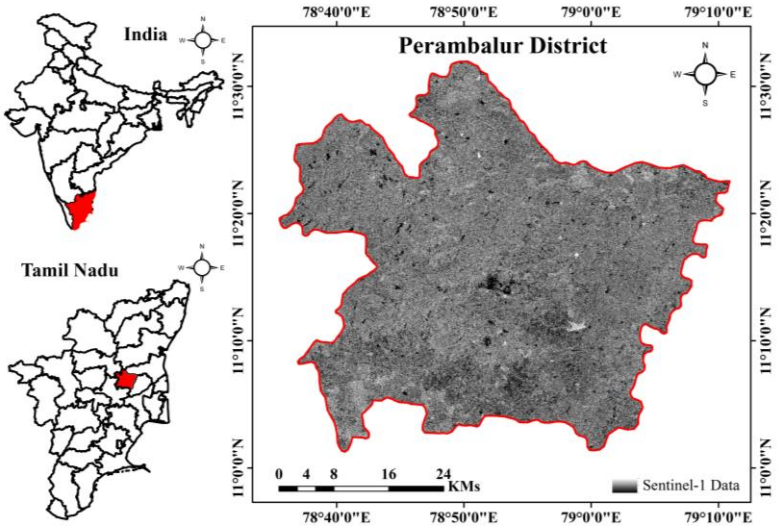

Figure 1. Study area map of the Perambalur District, India.

2.3. Spatial Model for Soil Metrics

A moisture content response to SAR data consists of both soil moisture and vegetation moisture shown in eq.1. ISVI is the empirical model that accounts for vegetation in soil moisture estimation by multiplying the ISVI index with total moisture shown in eq.2 [17]. Subtracting vegetation moisture from total moisture yields soil moisture from eq.3. An empirical simulation "Soil Textural Index (STI)" based on the surface under study has a semi-saturated condition with constant roughness shown in eq.4 [13]. A density space di-electric model estimates soil salineness. According to the database, the real part (ϵ') of field saline soil from total salt is higher than the imagined part (ϵ"), while the imaginary part from fluoride soil is less than the total salinity. This shows that fluoride dielectric loss is smaller than soil salts. The distinction between fluoride and other components helps us distinguish them.

The absence of free water makes estimating the imaginary part of dielectric loss difficult. Thus, high saline conditions are used to calculate fluoride content. High saline-high fluoride and high saline-low fluoride soil sample data were measured in the lab. A high saline low fluoride soil is considered non-fluoride saline; Fluoride has a minor influence, while high saline high fluoride has a greater effect and helps define a dielectric constant. The 2D plot between the real and imaginary parts of fluoride helps estimate conductance losses due to fluoride and can be quantified. An imaginary part due to soil fluoride is estimated as a function of real and imaginary parts of the dielectric constant and the tangent loss shown in eq.5. A linear relationship between in-situ soil fluoride and the imaginary part of fluoride shows fluoride values in mg/kg.

$$m_v^{tot} = \sqrt{(m^o_{vv-opt-max}(\theta) - m^o_{vv-opt-i}(\theta))^2 + (m^o_{vv-opt-i}(\theta))^2} \quad (1)$$

$$m_v^{veg} = m_v^{tot} * ISVI \quad (2)$$

$$m_v^{veg} = m_v^{tot} * ISVI \quad (3)$$

$$\text{Soil Textural Index}_{\text{i}}\ (\text{STI}_i) = \frac{(m_{vi}^{soil} - m_{vmin}^{soil})}{(m_{vmax}^{soil} - m_{vmin}^{soil})} \quad (4)$$

$$\epsilon_f^{"} = (\epsilon_{ns-SAR} - \epsilon_{s-SAR})\cos\theta - \left[\frac{\sqrt{(\sigma_{vv-max} - \sigma_{vv-i})^2 + STI^2}}{\cos\left[\tan^{-1}\left(\frac{\epsilon_{field-max}}{2D-SDM_{(NS)max}}\right)\right]}\right]\sin(\theta) \quad (5)$$

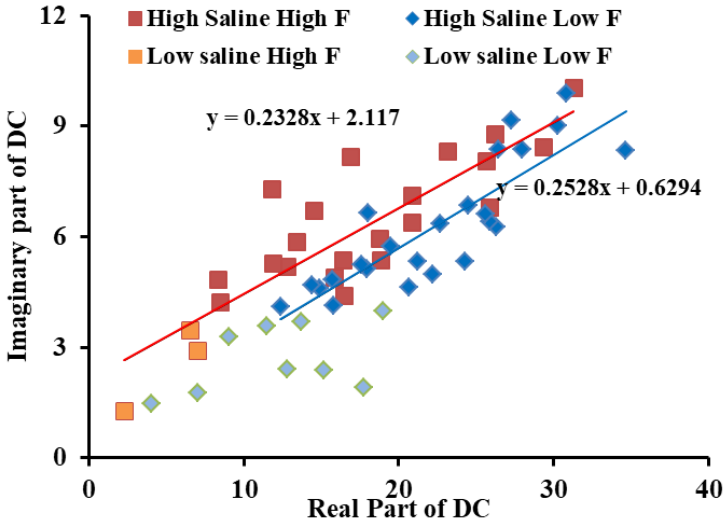

Figure 2. Tangent loss between real and Imaginary part of dielectric constant.

3. Result and Discussion

3.1. Soil Moisture and Textural Index

This study solely considers polarisation and ignores temperature in soil moisture evaluation. Polarisation is difficult to dry soil below 10% moisture, resulting in overestimation. However, co-polarization works well for soil moisture increases of 10%–50%. A statistical examination for validation demonstrates that the SAR data product agrees with an R^2 of 0.83. In the upper 30%, soil and field moisture match. Due to confined water, the bottom region from 0 to 10% was difficult to anticipate. The soil textural index (STI) showed sand and clay percentages by moisture content and grain size-related porosity. The range of STI is 0.1 to 0.5, indicating that the research area has 50% to 75% clay soil and 34% to 50% sand. Clay soil badly affects soil texture, and sandy soil is not gathered. An STI score of 0 to 0.18 indicates high clay (40%) and sand (60%), whereas 0.19 to 0.6 indicates low clay (30%) and high sand (70%). A number greater than 0.6 indicates more sand and less clay and is not considered in this study. Texture is an important soil study feature that affects bound and free water in salt mobilisation considering grain size *[18]*.

This study examines the significance of the Soil Texture Index (STI) as a metric that is influenced by both precipitation rate and soil grain-specific surface area. The STI plays a crucial role in enhancing the interactions between electrical charges and fluid particles. The soil texture range of 0-0.4 has a higher clay content and comparatively lower levels of silt and sand. The phenomenon of cavitation has an impact on the velocity and elevation of water, which is contingent upon the size of soil particles [19]. Hence, the Soil Texture Index (STI) demonstrates a reliable capacity to appropriately depict soil type and dielectric constant, however, its ability to accurately assess clay and sand fraction is limited. This study demonstrates that the real component exhibits a positive correlation with soil moisture, rising from 20 to 50. Similarly, the imaginary component also displays a positive relationship, increasing from 0 to 10. These findings contribute to our comprehension of the characteristics of bound and free water.

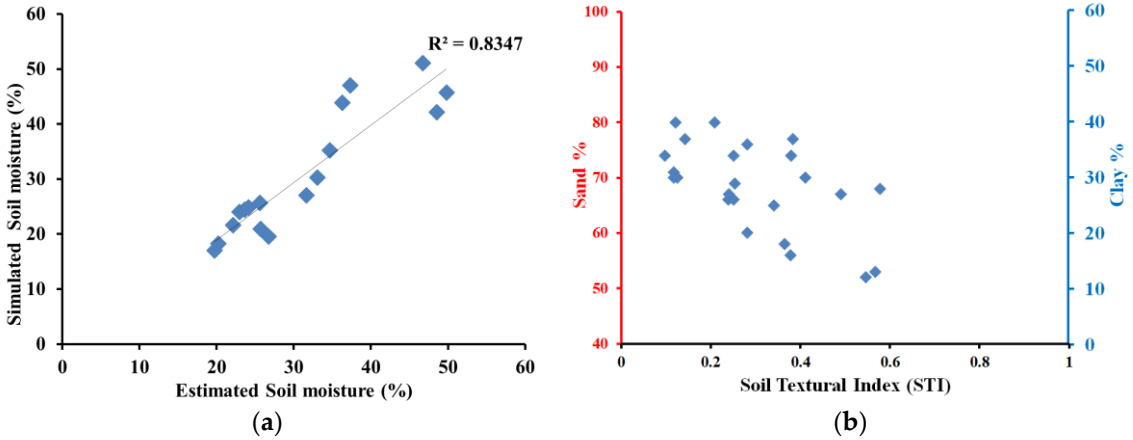

Figure 3. Validation and analysis of the (**a**) Soil moisture with field–observed values; (**b**) Proposed soil textural index.

3.2. Fluoride

Depending on ionic conductivity, soil pH is acidic or alkaline. A hypothetical chunk of fluoride-affected soil is segregated from tangent loss to distinguish it from non-fluoride soil. The dielectric constant of soil with total salts and fluoride is 0.81 and 0.86, respectively. A fluoride present in soil is range between 42 to 573 with an RMSE of 1.90 and positive bias of 0.35 with a significance level of 0.005.The model's accuracy is affected by over-estimating total salts and fluoride salts in the lower real and imaginary portions. Remove outliers to determine the model's accurate range and perform well in real and imaginary part ranges above 2. Fluoride ranges from 0 to 200 mg/kg, a model with an R^2 of 0.81 performs well, and STI values less than 0.2 are exaggerated in large amounts. STI is 0.2 to 0.4 is significantly exaggerated, and fluoride is 201 to 400 mg/kg. The plot shows a good agreement: the STI results are between 0.4 and 0.7, the range of fluoride is 401 mg/kg to 600 mg/kg, and the STI values above 0.7 are underestimated; the value is larger than 601 mg/kg. From that, soil texture plays a major role in fluoride contamination due to the amount of sand and clay.

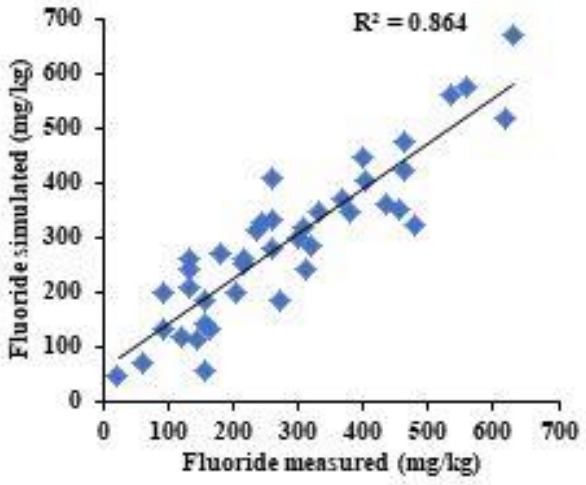

Figure 4. Validation of the simulated fluoride with estimated fluoride from conventional methods.

Additionally, clay presence increases fluoride content and vice versa, which may aid the F- estimate. The result showed that the simulated imaginary part of the dielectric constant owing to fluoride content with soil moisture content, identical to the DSDM model and exactly proportionate to soil salt concentration. The salinity caused by fluoride can be accurate and useful in determining its concentration. Fluoride in

low-moisture soil or soil with bound water cannot dissolve entirely. The more water in the soil, the more free ions migrate, increasing salinity and dielectric components. Counter ions travel mostly due to moisture. The link between electrical potential and mineral surface charges restricts clay soil mobility, confirming fluoride and C band frequency. Polarisation alone limits conductivity due to clay surface ionic concentration fluctuations.

Dry soil has a high dielectric constant because its volumetric water is minimal and its bound and free water influences are negligible. pH is crucial to soil salinity. An acidic soil pH range of 5 to 7 increases fluoride ion sorption and matches an anticipated imaginary part of the dielectric constant R^2 of 0.75. The collected soil fields lack an acidic soil pH range of 0 to 5, hence no investigations have been done. Alkaline soil in the sample ranges from 7 to 9. Clay soil is alkaline, thus positively charged ions sorb on its surface and reduce fluoride ion accumulation. Alkaline soils have an R^2 of 0.90 that matches the fictitious component. In clay soil, pH-dependent charges form uncompensated bonds controlled by inter-ions [20]. Quantifying mineral electrical characteristics requires soil pH. This part simulates the fluoride model to compare pH and evaluate dependability. Soluble fluoride components diminish soil sorption at lower pH [21]. Adding water to soil affects OH mobilisation, which controls pH from acidic to alkaline. Leaching solid fluoride components from soil to water-soluble F- rises. At high pH, pH-dependent negative charges on variably charged clay surfaces diminish soil F retention and raise F concentration. Thus, F sorption greatly depends on pH, and the most dominant soil for F-ion mobilisation is pH 4–6. Based on previous studies, acidic soil causes more ionic movement, so this study correlates geographically measured permittivity value with measured soil using straight-line fitting. Prototypical soils with varied silt and low sand content increase uncertainty.

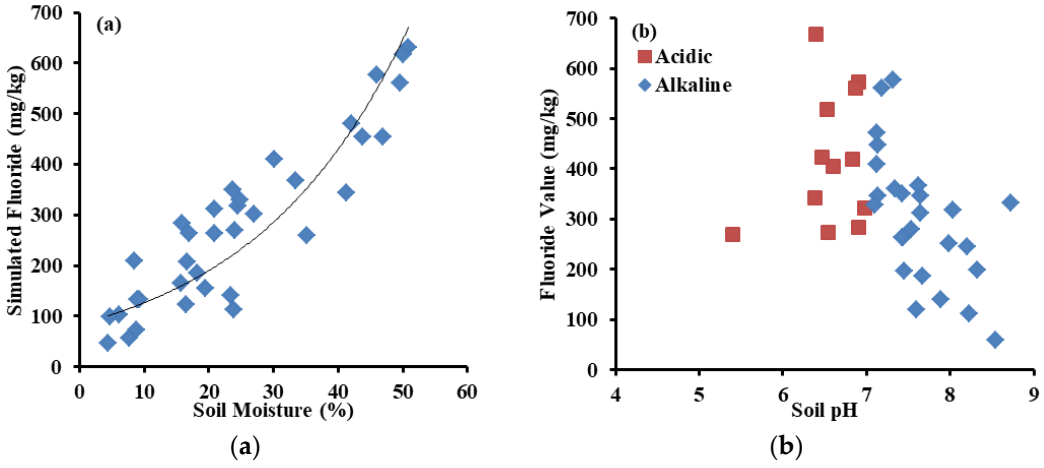

Figure 5. Response of the estimated fluoride to: (**a**) Soil moisture; (**b**) Soil pH .

4. Conclusion

Fluoride increases clay soil dielectric loss due to dry to saturated soil moisture. This showed that soil moisture affected the dielectric constant and could be used to forecast it over broad areas of time. Tangent loss increases with the moisture level in clay soil, indicating tangent loss (θ) can identify F^- salt content. Soil with low tanδ and high ϵ_i moisture has dielectric characteristics similar to pure water. Future aspects should include modifying the soil moisture model to handle the problem in dry situations with polarization. Second, login polarisation and conductivity loss cause dielectric losses. The login polarisation must be considered in the world, and conductivity loss affects salinity.

Author Contributions: The first author created the fundamental concept and methodology, conducted the field and laboratory tests, statistically analysed, visualised, and prepared the manuscript. The second author validated, evaluated, supervised, and edited the manuscript.

Funding: This research received no external funding.

Institutional Review Board Statement: Not Applicable

Informed Consent Statement: Not Applicable

Data Availability Statement: Data will be shared on request.

Acknowledgments: The authors express their gratitude to the SRMIST, Kattankulathur for their assistance and exceptional laboratory resources in facilitating this study. The provision of complimentary data dissemination by the European Space Agency is highly valued.

Conflicts of Interest: The authors do not have any conflict of interest in our manuscript.

References

1. X Unde, M.P., Patil, R.U. and Dastoor, P.P. The untold story of fluoridation: Revisiting the changing perspectives. *Indian journal of occupational and environmental medicine,* **2018**, 22(3), p.121.
2. Singh, G., Kumari, B., Sinam, G., Kumar, N. and Mallick, S. Fluoride distribution and contamination in the water, soil and plants continuum and its remedial technologies, an Indian perspective–a review. *Environmental Pollution*, **2018**, 239, pp.95-108.
3. Yardımcı, B., Uzer, A. and Apak, R. Spectrophotometric fluoride determination using St. John's wort extract as a green chromogenic complexant for Al (III). *ACS omega*, **2022**, 7(49), pp.45432-45442.
4. Zhu, L., Zhang, H.H., Xia, B. and Xu, D.R. Total fluoride in Guangdong soil profiles, China: spatial distribution and vertical variation. *Environment International*, **2007**, 33(3), pp.302-308.
5. Singh, G., Sinam, G., Kriti, Pandey, M., Kumari, B. and Kulsoom, M. Soil pollution by fluoride in India: distribution, chemistry and analytical methods. *Environmental Concerns and Sustainable Development*: *Volume 2: Biodiversity, Soil and Waste Management*, **2020**, pp.307-324.
6. Shahabfar, A., Ghulam, A. and Eitzinger, J. Drought monitoring in Iran using the perpendicular drought indices. *International Journal of Applied Earth Observation and Geoinformation*, **2012**, 18, pp.119-127.
7. Hazaymeh, K. and Hassan, Q.K. A remote sensing-based agricultural drought indicator and its implementation over a semi-arid region, Jordan. *Journal of Arid Land*, **2017**, 9, pp.319-330.
8. Chandrasekar, K., Sesha Sai, M.V.R., Roy, P.S. and Dwevedi, R.S. Land Surface Water Index (LSWI) response to rainfall and NDVI using the MODIS Vegetation Index product. *International Journal of Remote Sensing*, **2010**, 31(15), pp.3987-4005.
9. Zhang, X., Zhang, H., Wang, C., Tang, Y., Zhang, B., Wu, F., Wang, J. and Zhang, Z. Soil moisture estimation based on the distributed scatterers adaptive filter over the QTP permafrost region using sentinel-1 and high-resolution TerraSAR-X data. *International Journal of Remote Sensing*, **2021**, 42(3), pp.902-928.
10. Kornelsen, K.C. and Coulibaly, P. Advances in soil moisture retrieval from synthetic aperture radar and hydrological applications. *Journal of Hydrology*, **2013**, 476, pp.460-489.
11. Yu, F. and Zhao, Y. A new semi-empirical model for soil moisture content retrieval by ASAR and TM data in vegetation-covered areas. *Science China Earth Sciences*, **2011**, 54, pp.1955-1964.
12. Mialon, A., Richaume, P., Leroux, D., Bircher, S., Al Bitar, A., Pellarin, T., Wigneron, J.P. and Kerr, Y.H. Comparison of Dobson and Mironov dielectric models in the SMOS soil moisture retrieval algorithm. *IEEE Transactions on Geoscience and Remote Sensing*, **2015**, 53(6), pp.3084-3094.
13. Ravi, K.P. and Periasamy, S. Integrated SAR simulation to categorize the stressed and salt-tolerant crops using Sentinel-1 data. *Geocarto International*, **2022**, 37(13), pp.3659-3678.
14. Jacob, M.V. Low temperature microwave characterisation of lithium fluoride at different frequencies. Science and Technology of Advanced Materials, **2005**, 6(8), pp.944-949.
15. Singh, B., Dolk, M.M., Shen, Q. and Camps-Arbestain, M. Biochar pH, electrical conductivity and liming potential. *Biochar: A guide to analytical methods*, **2017**, 23.
16. Pagliano, E., Meija, J., Ding, J., Sturgeon, R.E., D'Ulivo, A. and Mester, Z. Novel ethyl-derivatization approach for the determination of fluoride by headspace gas chromatography/mass spectrometry. *Analytical chemistry*, **2013**, 85(2), pp.877-881.
17. Krishnan, V., Periasamy, S. and Ravi, K.P. Integrated SAR Vegetation Index for Rabi And Kharif Crops. *In IGARSS 2022-2022 IEEE International Geoscience and Remote Sensing Symposium,* **2022,** *(pp*. 6406-6409). IEEE.
18. Újvári, G., Kok, J.F., Varga, G. and Kovács, J. The physics of wind-blown loess: Implications for grain size proxy interpretations in Quaternary paleoclimate studies. *Earth-Science Reviews*, **2016**, 154, pp.247-278.
19. Jie, S.U.N., Xinfeng, G.E., Dongdong, C.H.U. Zhang, L., Han, M.E.N.G. and Zheng, Y. Effects of sediment diameter and concentration on cavitation characteristics and mechanism. *Tribology International*, **2022**, 171, p.107543.
20. Li, X.,. Developing highly efficient oxygen evolution reaction electrocatalysts by electronic structure regulation on transition metal oxides, **2020**.
21. Onipe, T., Edokpayi, J.N. and Odiyo, J.O. Geochemical characterization and assessment of fluoride sources in groundwater of Siloam area, Limpopo Province, South Africa. *Scientific Reports*, **2021**, 11(1), p.14000.